Am J Nucl Med Mol Imaging 2014;4(4):324-332
www.ajnmmi.us /ISSN:2160-8407/ajnmmi0000229

Original Article

Targeting histone deacetylase in lung cancer for early diagnosis: ^{18}F-FAHA PET/CT imaging of NNK-treated A/J mice model

Wayland Tang[1], Sharon A Kuruvilla[1], Valentin Galitovskiy[3], Min-Liang Pan[1], Sergei A Grando[2,3], Jogeshwar Mukherjee[1,3]

[1]Preclinical Imaging, Department of Radiological Sciences, [2]Department of Dermatology, [3]Cancer Center and Research Institute, University of California, Irvine, California 92697, USA

Received March 13, 2014; Accepted April 9, 2014; Epub June 7, 2014; Published June 15, 2014

Abstract: Elevated levels of histone deacetylases (HDACs) have been indicated in the development of some cancers. HDAC has been imaged using ^{18}F-FAHA and may serve as a marker to study epigenetics. We report evaluation of ^{18}F-FAHA as a probe in the early diagnosis of lung cancer using ^{18}F-FAHA PET/CT studies of A/J mice treated with NNK. ^{18}F-FAHA radiosynthesis was carried out in specific activity of ~2 Ci/μmol. A/J mice were divided into 2 groups: 1. Controls; 2. NNK treatment group with NNK (100 mg/kg, ip, weekly for 4 wks). Mice were injected 100-200 μCi i.v. ^{18}F-FAHA and then scanned in Inveon PET/CT under anesthesia using 2.0% isoflurane. Midbrain, cerebellum and brainstem uptake of ^{18}F-FAHA was displaced by the known HDAC inhibitor, suberanilohydroxamic acid (SAHA) with less than 10% activity remaining. CT revealed presence of lung nodules in 8 to 10-month old NNK mice while control mice were free of tumors. Little uptake of ^{18}F-FAHA was observed in the control mice lungs while significant ^{18}F-FAHA uptake occurred in the lungs of NNK-treated mice with tumor/nontumor >2.0. Ex vivo scans of the excised NNK and control mice lungs confirmed presence of extensive amounts of lung nodules seen by CT and confirmed by ^{18}F-FAHA in the NNK mice with tumor/nontumor >6.0. Our preliminary imaging studies with A/J mice lung cancer model suggest ^{18}F-FAHA PET may allow the study of epigenetic mechanisms involved in NNK-induced tumorigenesis in the lungs.

Keywords: Lung cancer, histone deacetylase, ^{18}F-Nifene, ^{18}F-FAHA, ^{18}F-FDG, NNK, A/J mice, PET/CT

Introduction

Smoking produces *N*-nitrosamines, *N*-nitrosodimethylamine, *N*-nitrosopyrrolidine, *N'*-nitrosonornicotine and 4-(methylnitrosamino)-1-(3-pyridyl)-1-butanone (NNK), and exposure to these products lead to lung cancer [1]. NNK has been shown to induce pulmonary adenocarcinomas (PAC) in rodents where high incidences occurred especially in lungs of strain A/J progeny (24 wk) [1]. Bioactivation of NNK in the lung to form keto acid is catalyzed by hemoglobin [2]. NNK causes genetic changes associated with hallmarks of malignant transformation and tumor growth [3].

Chromatin structure is established through ionic interactions between positively charged histone tails and negatively charged DNA backbone, whereby gene expression is regulated through post-translational modification of amino acid residues on the histone tails [4, 5]. To maintain normal cellular function, gene expression is tightly regulated through reversible modification of histone proteins carried out by histone deacetylases (HDACs) and histone acetyltransferases (HATs). HATs weaken this interaction through acetylation of histones to neutralize the charge leading to a more open chromatin structure and allowing for gene expression, whereas the opposing actions of HDACs deacetylase causes the histones to re-establish the positive charge leading to a closed chromatin structure and causing gene silencing [4].

There are four classes of HDACs (Classes I-IV). Class I HDACs are mainly found in the cell nucleus and target mostly histones whereas Class II HDACs target histone and nonhistone proteins

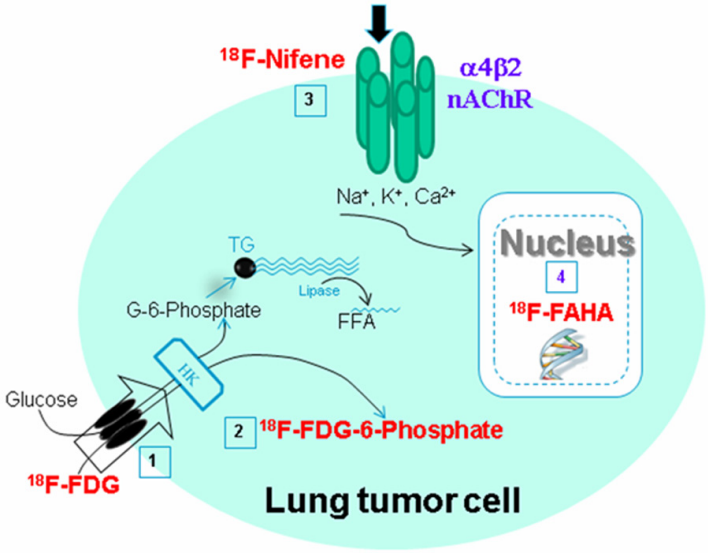

Figure 1. A scheme depicting the radiotracer targeting in a lung cancer cell. ^{18}F-FDG (1) uptake into the cell through the glucose transporter results in ^{18}F-FDG-6-phosphate (2) in the cytoplasm as a measure of glucose metabolic rate of the tumor cell. ^{18}F-Nifene (3) binding to the cell-membrane bound α4β2 nicotinic receptor measures the overexpression of the receptor in the tumor cell. ^{18}F-FAHA (4) uptake in the nucleus measures histone deacetylase upregulation in the tumor cell.

and are mostly found in the cytoplasm but are able to shuttle into the nucleus. Class IV HDACs share characteristics of both Classes I and II, and Class III HDACs are NAD^+-dependent and have roles different from the aforementioned HDAC classes [4, 6]. Atypical HDAC activities have been shown to play pivotal roles in the regulation of many hallmarks of cancer including tumor suppressor silencing and aberrant cell-cycle control. More importantly, high levels of HDACs have been indicated in various types of cancers, and inhibition of HDAC activity has been shown to activate pathways that induce cell cycle arrest, apoptosis and autophagy in cancer cells [4-7]. Deacetylation of nonhistone proteins by HDACs has also been shown to have effects on pathways related to tumor development and survival [4].

We have previously reported the use of ^{18}F-FDG for measuring glucose metabolism and ^{18}F-nifene for assessing α4β2 nicotinic receptors in the evaluation of the NNK-induced lung tumors in A/J mice as shown in **Figure 1** [8]. More recently, HDACs have been found to be involved in lung cancer and are being targeted for potential therapy [9, 10]. Therefore, HDACs may be a potential target in NNK-induced tumorogenesis since genetic changes have been observed [3].

Identification of potent HDAC inhibitors is important for development of anticancer therapy. One HDAC inhibitor, suberoylanilide hydroxamic acid (SAHA; **Figure 2**) also known as Vorinostat, has been approved for treatment of cutaneous T-cell lymphoma (CTCL) [4, 5, 7]. The structural commonalities shared by the PET agent 6-(^{18}F-fluoroacetamido)-1-hexanoicanilide (^{18}F-FAHA; **Figure 2**) and SAHA have suggested the use of ^{18}F-FAHA as a potential HDAC imaging agent [11, 12]. ^{18}F-FAHA has been used as a probe for imaging HDACs, including imaging studies in human breast carcinoma, xenografts in rats, human glioblastoma multiforme and baboon brain [13, 14].

Here we report evaluation of ^{18}F-FAHA for imaging HDACs as a potential imaging probe for lung cancer epigenetic mechanisms involved in NNK-induced tumorigenesis in mice lungs. Whole body ^{18}F-FAHA PET/CT imaging was carried out in normal mice. Subsequently, ^{18}F-FAHA PET/CT imaging was carried out in control and NNK-treated A/J mice for evaluation of uptake in the lungs. Ex vivo imaging of the lungs was carried out after the in vivo PET/CT.

Materials and methods

NNK lung model

The protocol for the lung tumor model was the same as previously described in the ^{18}F-nifene study [8]. Female strain A/J mice, 6-8 weeks old, were purchased from Jackson Laboratories (Bar Harbor, ME) and are known to develop lung tumors when exposed to tobacco nitrosamines [15]. All animals were housed in polypropylene boxes with *ad libitum* access to food and water, and conventional bedding material. Mice were treated in accordance to National Institutes of Health guidelines and as approved by the Institutional Animal Care and Use Committee of the University of California, Irvine. Mice were divided into an experimental group and a control group. Experimental mice were treated with NNK by subcutaneous injection of 100 μl in the upper back at a dose of 100 mg/kg once a week for four weeks. NNK was dissolved in

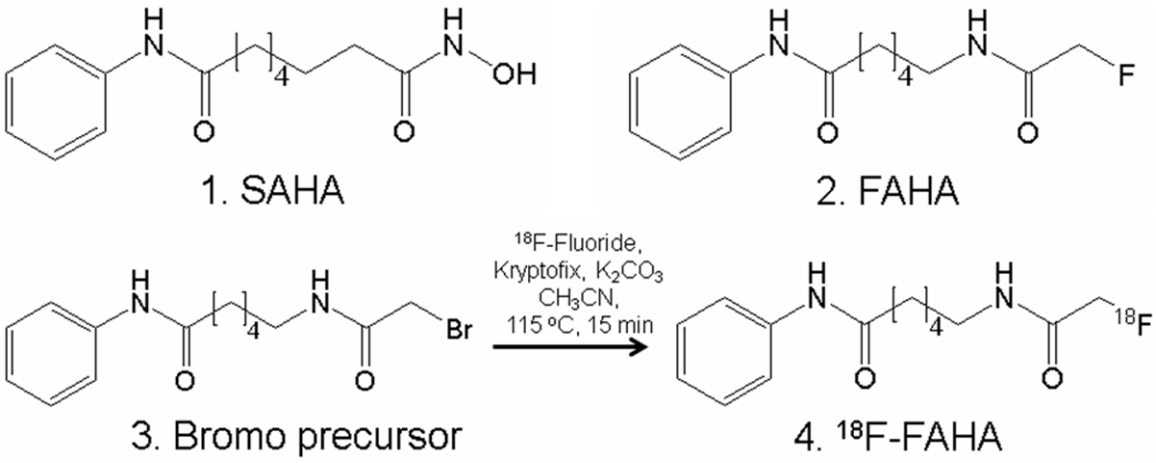

Figure 2. Structural similarities of SAHA and ^{18}F-FAHA. (1). Chemical structure of SAHA (2). Chemical structure of FAHA. (3). Bromo-precursor for radiolabeling with ^{18}F-fluoride for radiosynthesis of ^{18}F-FAHA (4). 6-(^{18}F-fluoroacetamido)-1-hexanoicanilide (^{18}F-FAHA).

DMSO in 10x concentration and diluted in corn oil to final concentration. Treatment control mice were injected with the same solution without NNK. Lung tissue sections from control and NNK-treated A/J mice were obtained following PET/CT scans (after a 24-hr period once the fluorine-18 radioactivity had decayed away) as described previously [8].

Radiosynthesis of ^{18}F-FAHA

Synthesis of FAHA 2 and radiosynthesis of ^{18}F-FAHA 4 was carried out in automated CPCU using ^{18}F-fluoride and reacting it with bromo-precursor 3 at 115°C for 15 mins (prepared and characterized using methods reported in [11]; **Figure 2**). ^{18}F-FAHA was obtained in 5% radiochemical yield after reverse-phase HPLC purification using 40% CH_3CN:60% phosphate buffer (retention time of bromo-precursor was 8.2 mins and ^{18}F-FAHA was 7.6 mins). Specific activity was >2 Ci/μmol [11]. The collected fraction was taken to near dryness *in vacuo*. The final formulation of ^{18}F-FAHA was carried out using approximately 2 to 5 mL of 0.9% saline followed by filtration through a membrane filter (0.22 μm) into a sterile dose vial for use in the PET studies.

PET and CT imaging

In study 1 involving control vs. NNK groups, three mice were used for the control group and three mice were used for the NNK group for a total of six mice (8 to 10 months post-NNK treatment). All the subjects were fasted 24 hours prior to PET imaging. In study 2 involving control mice and SAHA pre-injection with ^{18}F-FAHA, a total of three mice were used. All mice were induced with 4% isoflurane and maintained on 2-2.5% isoflurane in preparation for the scans. Whole body scans were performed using Inveon Multimodality (MM) CT scanner (Siemens) and Inveon dedicated PET scanner for a total of 30-45 min. CT images of the mice were obtained with a large area detector (4096 x 4096 pixels, 10 cm x 10 cm field-of-view). The CT projections were acquired with the detector-source assembly rotating over 360 degrees and 720 rotation steps. A projection bin factor of 4 was used in order to increase the signal to noise ratio in the images. The CT images were reconstructed using cone-beam reconstruction with a Shepp filter with cutoff at Nyquist frequency resulting in an image matrix of 480 x 480 x 632 and a voxel size of 0.206 mm. Longitudinal CT studies were analyzed using Inveon Research Workplace (IRW, Siemens Medical Solutions, Malvern, PA) software. Volumes of interest (3D VOIs) were drawn manually on the lungs of control and NNK-treated mice. VOIs were drawn as irregular contours on the high resolution CT images, and tumors were calculated by using the segmentation function in the IRW software.

Mice were injected with 100-200 μCi ^{18}F-FAHA *via* tail vein under anesthesia. The animals were then placed in the mouse chamber and were positioned in the Inveon Multimodality CT/PET scanner. The Inveon PET/CT was switched

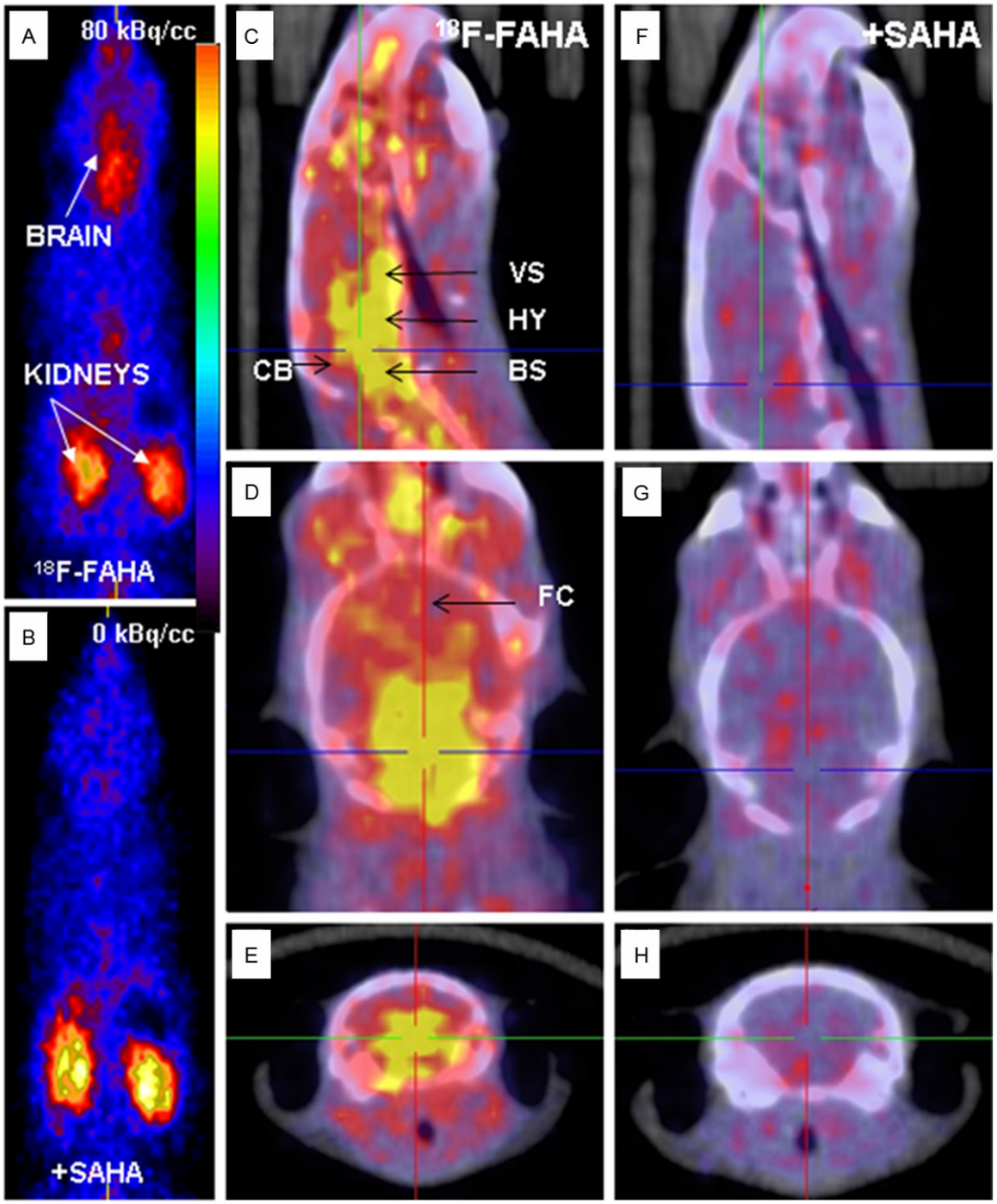

Figure 3. ^{18}F-FAHA binding in Control A/J Mice. A. Whole body PET in control mouse displays high ^{18}F-FAHA uptake in the brain and kidneys. B. Whole body PET in SAHA pre-injected mouse shows only in the kidneys with no uptake in the brain. C-E. PET/CT of A/J mice head showing high uptake in the brain indicated in yellow regions (VS: ventral striatum; HY: hypothalamus; CB: cerebellum; BS: brain stem; FC: frontal cortex). F-H. Little uptake in the brain is shown in SAHA pre-injected mouse.

to the "docked mode" for combined PET/CT experiments. A CT scan was then obtained for reconstruction of the PET data and further analysis of the PET/CT data. Duration of the PET scan was typically 30 min and was timed to start 60 min post-injection of ^{18}F-FAHA. The images were reconstructed using Fourier rebinning and 2-dimensional filtered back-projection

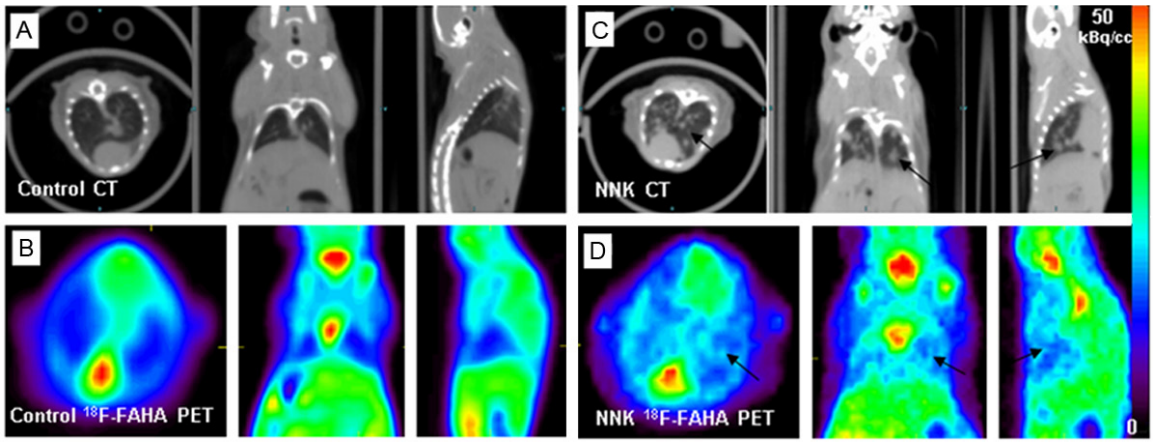

Figure 4. ^{18}F-FAHA binding in Lungs. A. CT of control mice with no visualization of lung tumor nodules; B. ^{18}F-FAHA PET with no visualization of lung tumor nodules; C. NNK-treated mice display multiple regions of lung tumor growth (arrows). D. ^{18}F-FAHA PET in NNK-treated mice display multiple regions of lung tumor growth (arrows).

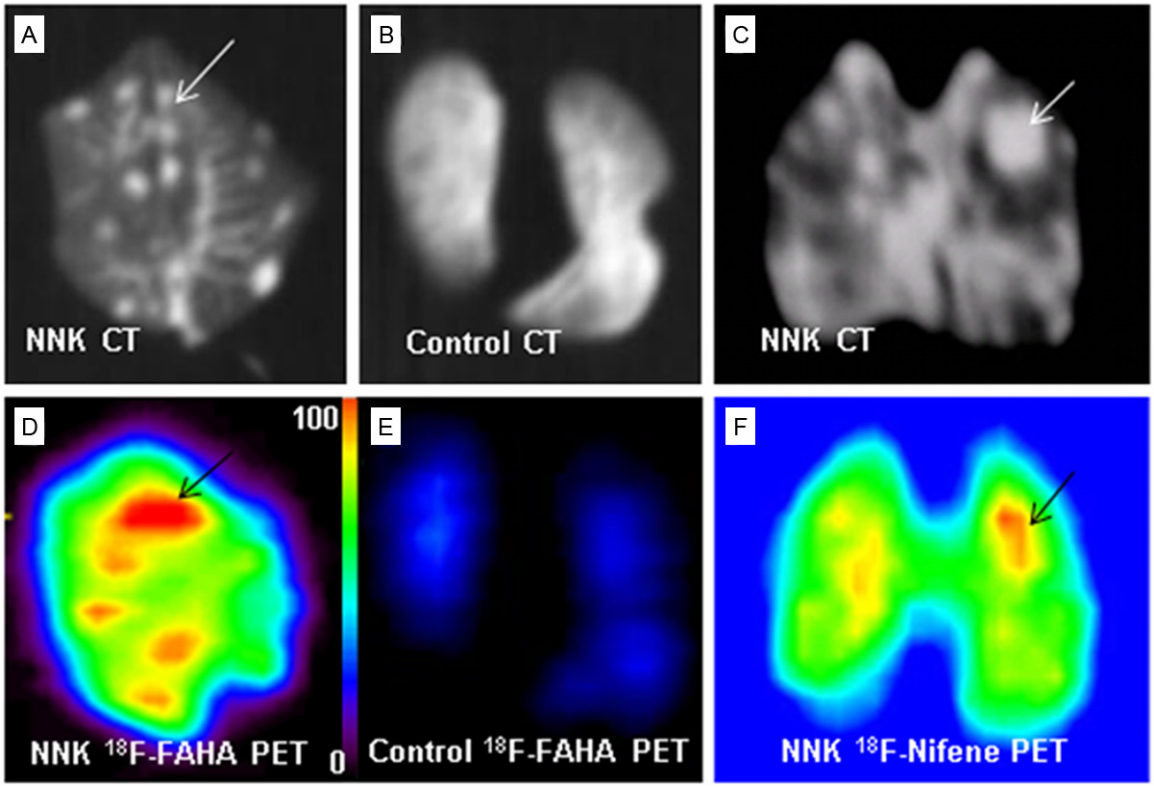

Figure 5. Ex vivo PET/CT imaging studies. (A, C) CT images show distinct lung nodules in NNK treated mice (arrows) and (B) lung free of tumors in the control group. (D) PET shows high ^{18}F-FAHA uptake at tumor sites indicated by arrows; (E) Shows no activity in the lungs of the control group indicated by blue regions; (F) PET shows high ^{18}F-Nifene uptake at tumor sites indicated by arrows.

(2D FBP) method (ramp filter and cutoff at Nyquist frequency) with an image matrix of 128 x 128 x 159, resulting in a pixel size of 0.77 mm and a slice thickness of 0.796 mm. The PET data for ^{18}F-FAHA were analyzed as tumor to nontumor ratios. Similar to previously described methods [8], the VOIs were first delineated visually by contouring the ^{18}F-FAHA activity that was clearly above normal background activity in the lungs. These areas were confirmed in the

corresponding CT of each animal. The amount of ^{18}F-FAHA activity in each VOI (in kBq/mL) of the tumor and areas of the lung that did not have any tumors (nontumor) was measured and confirmed using the corresponding CT scans of each individual animal. ^{18}F-FAHA uptake in the brain was computed in the brain of mice with and without pretreatment SAHA.

Ex vivo studies

After the ^{18}F-FAHA PET/CT scan, the mice under anesthesia were decapitated and the lungs were rapidly removed and frozen in dry ice. Whole lungs (from a control mouse and NNK-treated mouse treated with ^{18}F-FAHA) were placed in a hexagonal polystyrene weighing boat and covered with powdered dry ice and placed securely on the scanner bed. Scans (PET and CT) were acquired for 30 min of ^{18}F-FAHA containing lungs. Images were analyzed using the Acquisition Sinogram Image Processing (ASIPRO, Siemens Medical Solutions, Malvern, PA) and IRW software from Siemens Medical Solutions.

Results

Radiosynthesis of ^{18}F-FAHA

In this study, the synthesis of ^{18}F-FAHA was successfully carried out and was found to be consistent with previously reported methods [11]. High specific activity and radiochemical yields were obtained for in vivo studies. This allowed specific localization of ^{18}F-FAHA in brain areas known to have HDACs.

Brain PET and CT imaging

Prominent uptake of ^{18}F-FAHA in normal mice occurred in various brain regions as shown in **Figure 3A** while clearance was seen to occur predominantly from the kidneys. Various cerebral and cerebellar regions showed binding and was consistent with some observations in rodents and nonhuman primates as reported previously [13, 17]. Pre-injection of SAHA, a known inhibitor of HDAC and known to cross the blood-brain barrier, reduced the uptake of ^{18}F-FAHA significantly in various parts of the brain, as shown in **Figure 3B**. Activity in the kidneys was unaffected by SAHA treatment since the kidney is the excretory pathway of ^{18}F-FAHA. HDAC binding specificity was shown through PET assays via SAHA pre-injection. The standard uptake value, SUV for brain uptake in control mice was 1.40±0.20 and in the presence of SAHA the brain SUV went down to 0.19±0.10. Thus, control mice injected with ^{18}F-FAHA and SAHA exhibited a >85% reduction in brain ^{18}F-FAHA consistent with the dose-dependent study reported in nonhuman primates [14].

Lung PET and CT imaging

CT evaluation of both groups of A/J mice showed presence of lung nodules in the 8 to 10-month old mice of the NNK-treated group while no tumors were detected in the control group (**Figure 4**). The multiple tumors detected in the NNK-treated group were confirmed through post-mortem analysis in our previous report [8]. Confirmation of these results provides the basis for the NNK-induced A/J mice lung tumor model used in our study.

PET evaluation of A/J mice showed little ^{18}F-FAHA activity in the lungs of the control group (**Figure 4B**), unlike the high level of activity in the brain. The NNK-treated A/J mice showed high ^{18}F-FAHA activity at tumor sites in the lungs evident in all the 3 planes as seen in **Figure 4D**. These observations were consistent in all the animals that were studied with ^{18}F-FAHA. Quantitative analysis of ^{18}F-FAHA binding provided lung tumor to nontumor ratio of >2. In both NNK and control groups of A/J mice, high uptake was noticed in the kidneys due to the excretion pathway.

Ex vivo studies

After in vivo scans, ex vivo PET/CT scans of lungs were performed on two mice. Ex vivo CT studies confirm detection of lung nodules (**Figure 5A**) while the control lung did not exhibit any nodules or any significant amount of retention of ^{18}F-FAHA (**Figure 5C**). High uptake ^{18}F-FAHA was evident in the NNK-treated mice as seen in **Figure 5B** while the control mice lung had very low levels of ^{18}F-FAHA binding (**Figure 5D**). Quantitative analysis of ^{18}F-FAHA binding in ex vivo scans provided lung tumor to nontumor ratio of >6.

Discussion

There is emerging interest in the development of imaging methods in order to study epi-

Table 1. Quantitation of CT and PET Imaging in NNK-treated A/J Mice

Study	In Vivo PET/CT	Ex Vivo PET/CT	Measure of
CT[a,b]	>7 mm^3	na	Tumor volume
^{18}F-FDG[a]	<1.5[c]	>3[d]	Glucose metabolism
^{18}F-Nifene[a]	1.8-2.0[c]	>4[d]	α4β2 nAChR levels
^{18}F-FAHA	>2[e]	>6[f]	HDAC activity

Animals were scanned 8-10 months post-NNK treatment. [a]Data taken from [8] Galitovskiy et al., 2013; [b]*In vivo* measures of tumor volume in NNK-treated animals (n=3, data are mean ± SD, $p < 0.05$ for the three age groups); [c]Ratio of tumor/nontumor in NNK-treated animals in vivo; [d]Ratio of tumor/nontumor of *ex vivo* lung post-treatment measured using PET; [e]Ratio of tumor/nontumor ^{18}F-FAHA in NNK-treated animals in vivo; [f]Ratio of tumor/nontumor of *ex vivo* lung ^{18}F-FAHA post-treatment; na: not available.

genetics [18]. PET imaging agents are thus being pursued to study HDACs in this effort [19-21]. Currently, ^{18}F-FAHA is being used since it has exhibited properties in vivo which reflect measures of HDACs [11]. Consistent with recent findings of localization of ^{18}F-FAHA in the monkey brains [17, 18], significant binding of ^{18}F-FAHA occurred in the A/J mouse brain regions. Mid-brain regions including ventral striatum, hypothalamus, brain stem and areas within the cerebellum similar to the monkey brain findings were observed [17]. Similar to the monkey brain, the HDAC inhibitor SAHA was able to inhibit binding of ^{18}F-FAHA. Thus ^{18}F-FAHA is able to be selectively localized in areas of the brain of A/J mice expressing HDACs.

The use of ^{18}F-FDG in the diagnosis of lung cancer has been underway clinically using PET/CT. There is however a need to further improve the sensitivity of detection. Our previous work with the NNK-treated A/J mice examined the use of ^{18}F-nifene, a novel diagnostic marker for nicotinic α4β2 receptor [8]. Our results showed that there is an overexpression of this receptor in the lungs and PET studies showed greater localization of ^{18}F-nifene, both in vivo and ex vivo. For comparison, shown in **Figure 5C**, **5F** is the selective localization of ^{18}F-nifene in the lung tumor.

Since genetic changes have been implicated in lung cancer and in this model of lung cancer [3], our goal was to evaluate epigenetic effects using HDAC as the target [22], aside from the glucose metabolic activity (as measured by ^{18}F-FDG) and alterations in the nicotinic receptors (as measured by ^{18}F-nifene) shown in **Figure 1**. Due to the increasing role of histones in cancer, and in particular HDACs, it was considered to be a useful target. Recent work has shown a significant increase in the levels of HDACs in colorectal cancer with approximately a 100% increase in HDAC1, HDAC2, HDAC3, HDAC5 and HDAC7 [22]. Immunohistochemical expression of HDAC1, HDAC2 and HDAC3 progressively increased in benign, borderline and malignant ovarian tumors [23]. Using cigarette smoke condensate and lung cell lines, it has been recently shown that cigarette smoking may promote epithelial to mesenchymal transition, cell migration and invasion in non-small cell lung cancer through downregulation of E-cadherin which is mediated by histone deacetylation [24]. Therefore, we tested the hypothesis that ^{18}F-FAHA can visualize HDACs in lung tumors of NNK-treated A/J mice, thus enabling early diagnosis of lung cancer.

The ability of ^{18}F-FAHA to detect NNK-induced lung cancer in A/J mice was evident, compared to the very low retentions of ^{18}F-FAHA in lungs of control mice. Postmortem histopathological analysis of the lungs confirmed the presence of tumors [8]. The tumor/nontumor ratios within the same animals were >2, illustrating greater ^{18}F-FAHA binding to the tumors. An increased lung tumor uptake of ^{18}F-FAHA was confirmed by ex vivo studies of the excised lungs, showing the tumor/nontumor ratios >6. The ability to more clearly discern the tumor and nontumor regions in the ex vivo scans (**Figure 5**) compared to the in vivo scans (**Figure 4**) may attribute to the higher tumor/nontumor ratio in the former. Although the ex vivo CT of the lungs from the NNK-treated mice revealed large amounts of tumor nodules, in vivo CT was not as clearly discernible. This fact indicates that combining CT and PET increased sensitivity of detection of small lung tumors.

High levels of HDACs have been indicated in various types of cancers [25], and our findings vividly demonstrated that lung cancer cells in A/J mice abundantly express HDACs binding ^{18}F-FAHA. PET imaging studies using ^{18}F-FAHA in probing of HDACs in rat carcinoma xenografts have been reported, showing tumor to

muscle binding ratio of approx. 2, where radiotracer uptake was inhibited by SAHA [14]. Development of noninvasive imaging of HDACs in cancer may be of value in assessing the efficacy of treatment by emerging HDAC inhibitors [26].

Table 1 compares the use of the three radiotracers in this mice model of lung cancer. Amongst the three, ^{18}F-FDG provided the lower tumor-to-nontumor ratios both in vivo and ex vivo. This is suggestive of the higher uptake of ^{18}F-FDG in nontumor regions. An additional issue with ^{18}F-FDG in small animals is the interference from activity in the heart. The ratios in vivo of ^{18}F-nifene and ^{18}F-FAHA were comparable with ^{18}F-FAHA showing slightly higher ratios. Preliminary reports indicate that HDAC expression may be correlated with Ki-67 expression [23]. Further studies will have to be carried out in order to evaluate efficacy of the three radiotracers for early diagnosis of lung tumor in A/J mice.

Conclusion

The binding specificity of ^{18}F-FAHA to HDACs in NNK-induced lung tumors provides a valuable in vivo imaging probe. Further studies on ^{18}F-FAHA in tumor growth and ^{18}F-FAHA binding to a specific class and subtype of HDAC enzyme may provide specificity of binding. Although these are preliminary findings, our results show the potential of the use of ^{18}F-FAHA (or other HDAC markers) as a diagnostic radiotracer to understand the progression of lung cancer and for use in monitoring anticancer therapy.

Acknowledgements

This work was supported by the National Institute for Health Grant # R01 AG029479 (JM) and # R01 ES017009 (SAG). We would like to thank Alex Corches and Drs. Evegueni Sevrioukov and Cristian Constantinescu for technical assistance.

Disclosure of conflict of interest

The authors have no conflict of interest.

Address correspondence to: Dr. Jogeshwar Mukherjee, B138 Medical Sciences, University of California-Irvine, Irvine, CA 92697, USA. Tel: 949-824-2018; Fax: 949-824-2344; E-mail: j.mukherjee@uci.edu

References

[1] Zheng HC, Takano Y. NNK-Induced Lung Tumors: A Review of Animal Model. J Oncol 2011; 2011: 635379.

[2] Bedard LL, Smith GB, Reid KR, Petsikas D, Massey TE. Investigation of the role of lipoxygenase in bioactivation of 4-(methylnitrosamino)-1-(3-pyridyl)-1-butanone (NNK) in human lung. Chem Res Toxicol 2002; 15: 1267-1273.

[3] Gordon W, Galitovskiy V, Edwards R, Andersen B, Grando SA. The tobacco carcinogen nitrosamine induces a differential gene expression response in tumour susceptible A/J and resistant C3H mouse lungs. Eur J Cancer 2013; 49: 725-733.

[4] Atadja PW. HDAC inhibitors and cancer therapy. Prog Drug Res 2011; 67: 175-195.

[5] Lane AA, Chabner BA. Histone deacetylase inhibitors in cancer therapy. J Clin Oncol 2009; 27: 5459-5468.

[6] Marks PA, Xu WS. Histone deacetylase inhibitors: potential in cancer therapy. J Cell Biochem 2009; 107: 600-608.

[7] Rikiishi H. Autophagic and Apoptotic Effects of HDAC Inhibitors on Cancer Cells. J Biomed Biotechnol 2011; 2011: 830260

[8] Galitovskiy V, Kuruvilla SA, Sevrioukov E, Corches A, Pan ML, Kalantari-Dehaghi M, Chernyavsky AI, Mukherjee J, Grando SA. Development of novel approach to diagnostic imaging of lung cancer with ^{18}F-nifene PET/CT using A/J mice treated with NNK. J Cancer Res Ther 2013; 1: 128-137.

[9] Neal JW, Sequist LV. Exciting new targets in lung cancer therapy: ALK, IGF-1R, HDAC and Hh. Curr Treat Options Oncol 2010; 11: 36-44.

[10] Vendetti FP, Rudin CM. Epigenetic therapy in non-small-cell lung cancer: targeting DNA methyltransfereases and histone deacetylases. Expert Opin Biol Ther 2013; 13: 1273-1285.

[11] Mukhopadhyay U, Tong WP, Gelovani JG, Alauddin MM. Radiosynthesis of 6-([^{18}F]fluoroacetamido)-1-hexanoicanilide ([^{18}F]FAHA) for PET imaging of histone deacetylase (HDAC). J Label Comp Radiopharm 2006; 49: 997-1006.

[12] Reid AE, Hooker J, Shumay E, Logan J, Shea C, Kim SW, Collins S, Xu Y, Volkow N, Fowler JS. Evaluation of 6-([^{18}F]fluoroacetamido)-1-hexanoicanilide for PET imaging of histone deacetylase in the baboon brain. Nucl Med Biol 2009; 36: 247-258.

[13] Nishii R, Mukhopadhyay U, Yeh H, Soghomonyan S, Volgin SA, Alauddin M, Tong W, Gelovani J. Non-invasive imaging of histone deacetylase activity in human breast carcinoma xenografts in rats using positron emission

tomography (PET) with [^{18}F]-FAHA. J Nucl Med 2007; 48: 34 (abstract).
[14] Kuo JW, Su KH, Wu CY, Ho CH, Wang HE, Gelovani J, Liu RS. A simplified kinetic model for rat glioma using ^{18}F-FAHA. J Nucl Med 2011; 52: 1182 (abstract).
[15] Hecht SS, Isaacs S, Trushin N. Lung tumor induction in A/J mice by the tobacco smoke carcinogens 4-(methylnitrosamino)-1-(3-pyridyl)-1-butanone and benzo[a]pyrene: a potentially useful model for evaluation of chemopreventive agents. Carcinogenesis 1994; 15: 2721-2725.
[16] Yeh HH, Tian M, Hinz R, Young D, Shavrin A, Mukhapadhyaya U, Flores LG, Balatoni J, Soghomonyan S, Jeong HJ, Pal A, Uthamanthil R, Jackson JN, Nishii R, Mizuma H, Onoe H, Kagawa S, Higashi T, Fukumitsu N, Alauddin M, Tong W, Herholz K, Gelovani JG, Imaging epigenetic regulation by histone deacetylases in the brain using PET/MRI with ^{18}F-FAHA. Neuroimage 2013; 64: 630-639.
[17] Wang C, Schroeder FA, Hooker JM. Visualizing epigenetics: Current advances and advantages in HDAC PET imaging techniques. Neuroscience 2014; 264: 186-197.
[18] Seo YJ, Muench L, Reid A, Chen J, Kang Y, Hooker JM, Volkow ND, Fowler JS, Kim SW. Radionuclide labeling and evaluation of candidate radioligands for PET imaging of histone deacetylase in the brain. Bioorg Med Chem Lett 2013; 23: 6700-6705.
[19] Wang C, Eessalu TE, Barth VN, Mitch CH, Wagner FF, Hong Y, Neelamegam R, Schroeder FA, Holson EB, Haggarty SJ, Hooker JM, Design, synthesis, and evaluation of hydroxamic acid-based molecular probes for in vivo imaging of histone deacetylase (HDAC) in brain. Am J Nucl Med Mol Imaging 2013; 4: 29-38.
[20] Zeglis BM, Pillarsetty NV, Divilov V, Blasberg RA, Lewis JS. The synthesis and evaluation of N1-(4-(2[^{18}F]-fluoroethyl)phenyl-N8-hydroxyoctanediamide ([^{18}F]-FESAHA), a PET radiotracer designed for the delineation of histone deacetylase expression in cancer. Nucl Med Biol 2011; 38: 683-696.
[21] Hagelkruys A, Sawicka A, Rennmayr M, Seiser C. The biology of HDAC in cancer: The nuclear and epigenetic components. Handb Exp Pharmacol 2011; 206: 13-37.
[22] Stypula-Cyrus Y, Damania D, Kunte DP, Cruz MD, Subramanian H, Roy HK, Backman V. HDAC up-regulation in early colon field carcinogenesis is involved in cell tumorigenicity through regulation of chromatin structure. PLoS One 3013; 8: e64600.
[23] Hayashi A, Horiuchi A, Kikuchi N, Hayashi T, Fuseya C, Suzuki A, Konishi I, Shiozawa T. Type-specific roles of histone deacetylase (HDAC) overexpression in ovarian carcinoma: HDAC1 enhances cell proliferation and HDAC3 stimulates cell migration with downregulation of E-cadherin. Int J Cancer 2010; 127: 1332-1346.
[24] Nagathihalli NS, Massion PP, Gonzalez AL, Lu P, Datta PK. Smoking induces epithelial-to-mesenchymal transition in non-small cell lung carcinoma through HDAC-mediated downregulation of E-Cadherin. Mol Cancer Ther 2012; 11: 2362-2372.
[25] Witt O, Deubzer HE, Milde T, Oehme I. HDAC family: what are the cancer relevant targets. Cancer Lett 2009; 277: 8-21.
[26] West AC, Johnstone RW. New and emerging HDAC inhibitors for cancer treatment. J Clin Invest 2014; 124: 30-39.